Local and Fast Density Pump-out by ECRH in the LHD*)

Ryohei MAKINO[1)], Shin KUBO[1,2)], Takeshi IDO[1,2)], Kenji TANAKA[2)], Takashi SHIMOZUMA[2)], Yasuo YOSHIMURA[2)], Masaki NISHIURA[2)], Hiroe IGAMI[2)], Hiromi TAKAHASHI[2)], Akihiro SHIMIZU[2)] and Shinya OGASAWARA[1)]

[1)]*Department of Energy Engineering and Science, Nagoya University, Nagoya 404-8603, Japan*
[2)]*National Institute for Fusion Science, 322-6 Oroshi-cho, Toki 509-5292, Japan*

(Received 7 December 2012 / Accepted 30 May 2013)

A decrease in the electron density is observed during high-power heating, particularly in electron cyclotron resonance heating (ECRH). One possible mechanism is the increase in the number of trapped particles, which can enhance the radial particle flux, because ECRH accelerates electrons in a direction perpendicular to the magnetic field lines. To observe the effects of the production of trapped particles, high-power (1 MW) ECRH was applied at the ripple bottom of the magnetic field strength, where trapped particles are readily produced. A rapid local outward flux of electrons was first observed near the heating position shortly after ECRH injection. The outward flux is proportional to the electron density in the density range of 0.4×10^{19} to $0.8 \times 10^{19}\,\mathrm{m}^{-3}$. The inward electron flux was subsequently enhanced in the core region.

Keywords: density pump-out, ECRH, particle, transport, modulation, LHD

DOI: 10.1585/pfr.8.2402115

1. Introduction

Density pump-out has been observed in both tokamaks and helical systems [1] during high-power heating, particularly in electron cyclotron resonance heating (ECRH). It can also change the electric potential to positive [2]. The change in the radial electric field structure significantly affects confinement [3]. Changes in the electron density and radial electric field are the result of direct and indirect mutual interactions. Therefore, a good understanding of density pump-out phenomena is important for the control of the particle and heat transport and clarification of the role of the radial electric field in confinement.

One possible density pump-out mechanism is the production of trapped particles due to the acceleration of electrons in a direction perpendicular to the magnetic field lines by ECRH [4]. The deviation of the drift surfaces from the magnetic surfaces is larger for trapped particles than for passing particles. Furthermore, the center of the trajectory shifts with the transition from passing particles to trapped particles. This shift enhances the particle flux and decreases the electron density. The other mechanism proposed for density pump-out is confinement degradation due to the increase in the electron temperature gradient and the excitation of instabilities such as trapped electron modes [5]. Such a degradation of particle confinement is also observed in a tangential-negative-ion-based neutral-beam-heated plasma in the Large Helical Device (LHD) for low-density plasmas, where electron heating is dominant parallel to the magnetic field. This study reports the plasma's response to high-power ECRH applied at the ripple bottom of the magnetic field strength, where trapped particles are readily produced, enhancing the ECRH induced direct flux [6].

2. Experimental Setup

To observe the effects of the increase in the number of trapped particles, 1 MW 77 GHz ECRH was injected to the bottom of magnetic-ripple, where the effects of trapped particles are expected to be enhanced, in LHD. LHD parameters are a pole number of 2 and a toroidal period number of 10. The aspect ratio is about 6, and the minor radius a_{99} is about 0.6 m. Plasmas are sustained by negative-ion neutral beam injection (NBI) heating. Second-harmonic X(X2)-mode ECRH is used, because X2-mode ECRH increases the perpendicular speed more directly than the fundamental O-mode. In the Compact Helical System (CHS), X2-mode ECRH pumped out electrons more effectively than O-mode ECRH [1]. The power deposition profiles are set sharp at the minor radius $r_{\mathrm{eff}} = 0.19$ m on the outer side of the torus, as shown in Fig. 1. The magnetic field strength is adjusted to the second-harmonic resonance condition (1.375 T for 77 GHz) at the desired position. Helical systems have a ripple in the magnetic field strength caused by the toroidicity and the variation in the distance from the helical coils, which is called a helical ripple. Figure 2 (a) shows the magnetic field strength contour on the poloidal-toroidal plane and some magnetic field lines at $r_{\mathrm{eff}} = 0.19$ m. Figure 2 (b) presents the magnetic field strength at positions along the magnetic field line. The helical rip-

author's e-mail: makino.ryohhei@ms.nifs.ac.jp
*) This article is based on the presentation at the 22nd International Toki Conference (ITC22).

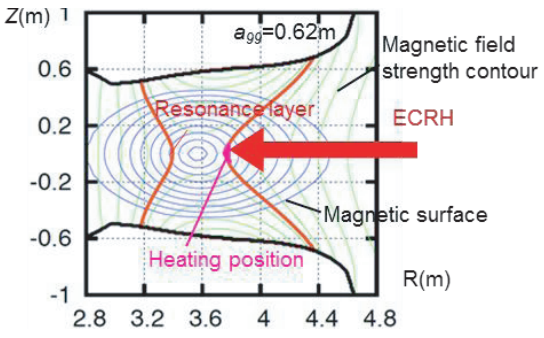

Fig. 1 Heating position and resonance layer on the cross section of torus. ECRH is injected to the magnetic ripple bottom at $r_{\rm eff} \sim 0.19$ m.

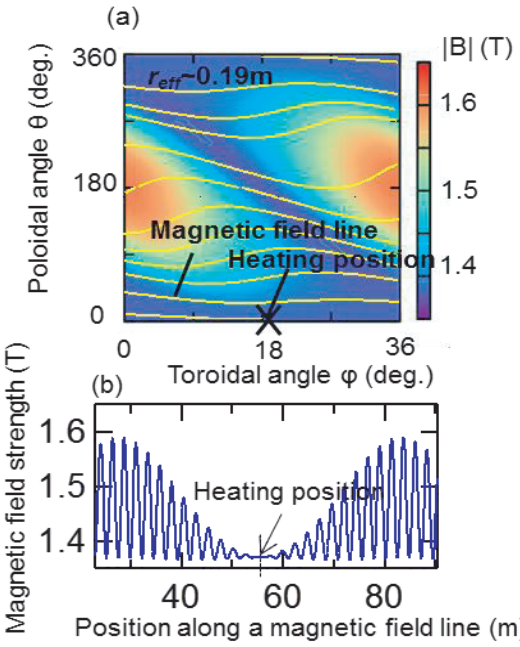

Fig. 2 (a) Magnetic field strength contour and field lines on the toroidal-poloidal plane at $r_{\rm eff} = 0.19$ m. (b) Magnetic field strength at positions along the magnetic field line.

ple is small at the outer side of the torus (near poloidal angle of 0°) for the magnetic axis at 3.6 m. ECRH was applied at the ripple bottom of the magnetic field strength along the magnetic field line at $r_{\rm eff} = 0.19$ m. ECRH was modulated as 100 ms on and 110 ms off. The electron density is about 0.6×10^{19} m^{-3}, which is below the cutoff density of X2-mode.

The line-integrated electron density was measured by multichannel far-infrared (FIR) laser interferometers. The local electron density was measured and estimated by both Thomson scattering (TS) and Abel-transformed FIR interferometer (Abel-FIR) data [7]. The electron temperature and electric potential were measured by using TS and a heavy-ion beam probe (HIBP), respectively.

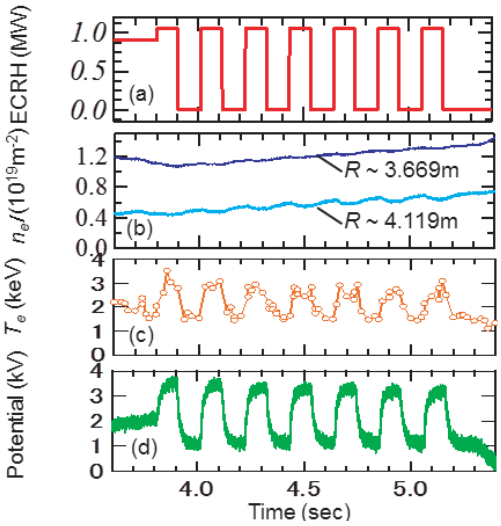

Fig. 3 Temporal evolution of (a) ECRH injection power, (b) line-integrated electron density from the upper to lower trace at R = 3.669 and 4.119 m measured by FIR laser interferometers, (c) electron temperature and (d) electric potential near the heating position ($r_{\rm eff} \sim 0.19$ m). Magnetic axis $R_{\rm ax}$ is 3.6 m. Minor radius a_{99} is 0.6 m.

3. Experimental Results

Figure 3 shows the temporal evolution of the line-integrated electron density, electron temperature, and electric potential measured by the FIR laser interferometers, TS and HIBP, respectively. The line-integrated electron density, electron temperature, and electric potential are modulated by ECRH. Figure 4 presents the electron density, electron temperature and electric potential profiles measured by TS and HIBP. These profiles were measured at the beginning and after 80 ms of ECRH injection. The electron temperature and electric potential were almost saturated at 80 ms after the ECRH injection beginning. To clearly observe the temporal response to ECRH, the measured data were superposed and averaged over all the ECRH modulation periods according to the relative time from the turn on/off phase (lock-in method). Figure 5 shows the line-averaged electron density measured by the FIR laser interferometers and locked by the ECRH modulation period. The line-averaged electron density was decreased by ECRH, which is usually reported for density clamping or pump-out. The local electron density locked by the ECRH modulation period is shown in Fig. 6. A rapid decrease in the electron density was observed near the heating position for 5 ms after the start of the bottom ECRH (Figs. 6 (a), (b)). The rapid decrease was observed by both Abel-FIR and TS. It occurred only inside the heating position ($r_{\rm eff} < 0.19$ m), as shown in Fig. 6 (c). After that, the electron density slowly increased with a time constant of about 40 ms. Figure 7 presents the temporal evolution of electric potential, electron temperature and electron density measured by HIBP, TS and Abel-FIR, respectively, inside the heating position, where the rapid decrease in the

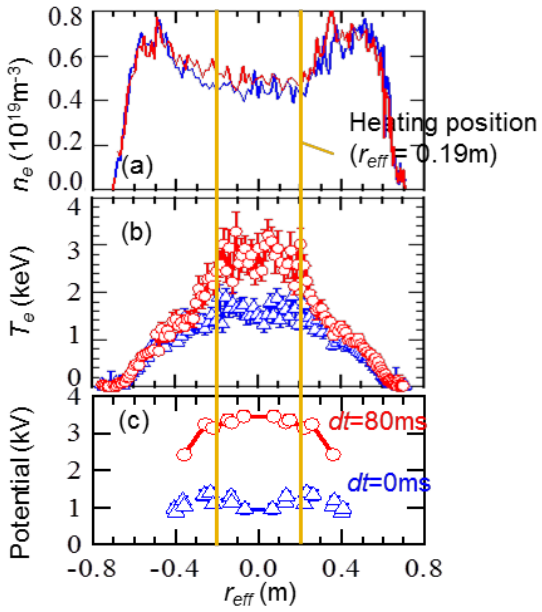

Fig. 4 Profiles of (a) electron density measured by TS, (b) electron temperature and (c) electric potential before ECRH injection (blue, dt = 0 ms) and 80 ms after ECRH injection (red, dt = 80 ms).

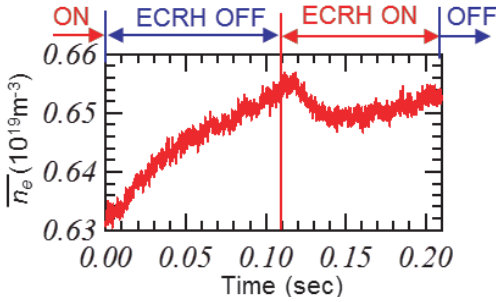

Fig. 5 Temporal evolution of line-averaged electron density locked by ECRH modulation period.

density was observed. A rapid increase in the electric potential was observed in phase with the rapid electron density decrease, both the increase and the decrease occurred only inside the heating position. The change in the electric potential is qualitatively consistent with the decrease in the electron density. The rapid increase in the electric potential and the decrease in the electron density indicate that ECRH enhances the outward flux of electrons shortly after the ECRH beginning.

4. Discussion

4.1 Particle flux induced by ECRH

The continuity equation of electrons can be written as

$$\frac{\partial n_e}{\partial t} = -\nabla \cdot \Gamma_e + S, \tag{1}$$

where S is the electron source term, and Γ_e is the electron flux. Because the electron flux can be experimentally

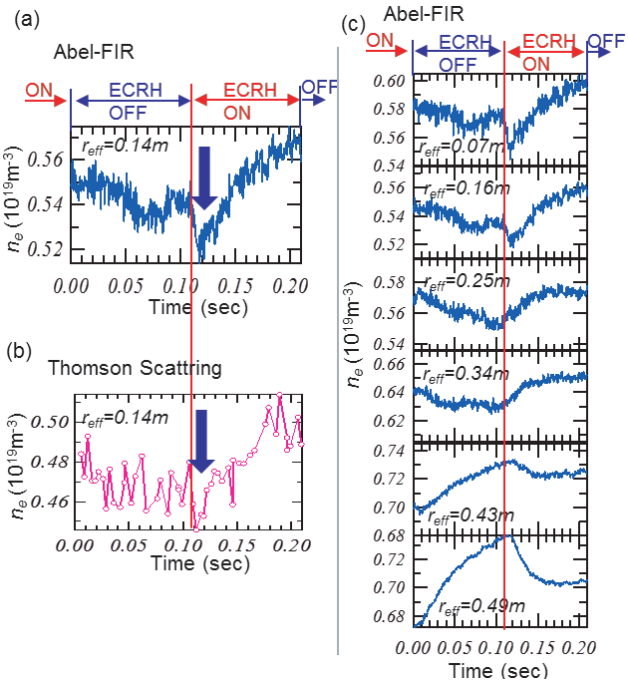

Fig. 6 Temporal evolution of electron density measured by (a) Abel-FIR and (b) TS near the heating position. (c) Electron density measured by Abel-FIR at each position. Heating position is r_{eff} ~ 0.19 m.

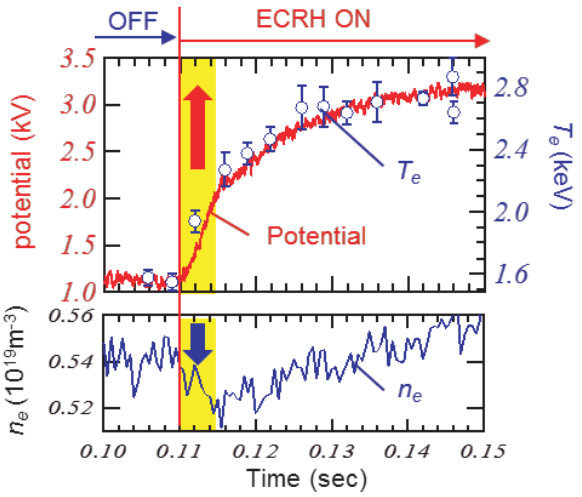

Fig. 7 Temporal evolution of electric potential, electron temperature T_e and electron density n_e near the heating positon (r_{eff} ~ 0.14 m).

deduced by equation (2).

$$\Gamma_e = -\frac{1}{r}\int_0^r r' \frac{\partial n_e}{\partial t} dr'. \tag{2}$$

The electron flux Γ_e can be expressed by equation (3) [8].

$$\Gamma_e = \Gamma_{NC} + \Gamma_{anom}(n_e, T_e, \nabla n_e, \nabla T_e, \nabla E_r, \ldots) + \Gamma_{ECRH}, \tag{3}$$

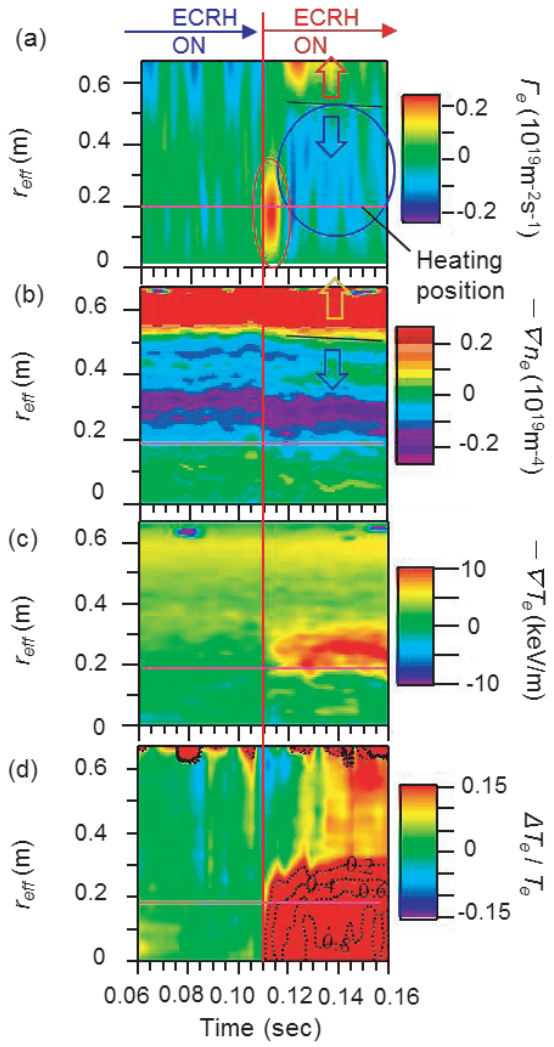

Fig. 8 (a) Electron flux estimated by Abel-FIR. (b) $-\nabla n_e$, (c) $-\nabla T_e$ estimated with n_e, T_e measured by TS. (d) Electron temperature increment ratio to that just after ECRH injection.

where Γ_{NC} is the neoclassical particle flux, Γ_{anom} is the anomalous particle flux, and Γ_{ECRH} is the particle flux enhanced by ECRH. The electron flux of neoclassical theory is written by equation (4) [9].

$$\Gamma_{NC} = -D_{e,n}\nabla n_e - n_e D_{e,T}\frac{1}{T_e}\nabla T_e - n_e D_{e,E}\frac{eE_r}{T_e}, \quad (4)$$

where $D_{e,n}$, $D_{e,T}$, and $D_{e,E}$ are diffusion coefficients, and E_r is the radial electric field. Figure 8 shows the temporal evolution of the profiles of Γ_e, the gradients of the electron density and temperature, and the increment ratio of the electron temperature from the beginning of ECRH. The electron flux Γ_e is deduced by equation (2) with the electron density estimated by Abel-FIR. The electron density gradient and temperature gradient were calculated with the electron density and temperature measured by TS.

The rapid local outward electron flux was observed near the heating position on a short time scale for 5 ms after the start of ECRH for the first time. In the case that the change in the outward particle flux is caused by the transition from passing particles to trapped ones, the outward flux is driven locally within time scales on the order of the transition time from passing particles to trapped ones and the transit time of trapped particles. In the second cyclotron resonance heating, the rate at which passing particles change to trapped ones can be deduced as equation (5) [4].

$$\frac{1}{\tau} = \frac{\dot{v}_\perp}{v_\perp} = \frac{P_{ab}}{2n_e T_e}, \quad (5)$$

where $v_\perp$ is the electron velocity perpendicular to the magnetic field lines, and P_{ab} is the absorbed ECRH power averaged on the magnetic surface. For a total absorbed ECRH power of $P_{tot} \sim 1$ MW, $n_e \sim 0.6 \times 10^{19}$ m^{-3}, $T_e \sim 2$ keV, power deposition location $r_{eff} \sim 0.19$ m, ECRH absorption depth $X_{ECRH} \sim 30$ mm, the magnetic axis $R_{ax} \sim 3.6$ m, the time constant of the transition is estimated as $\tau \sim 3$ ms by equation (5). Further, the transit time of the trapped particles is estimated to be about 10 ms [4].

From 8 ms after the start of ECRH, an inward electron flux was observed in the core region of the plasmas. In addition, an outward electron flux was observed in the peripheral region. These electron fluxes are in the same direction as $-\nabla n_e$ (Fig. 8 (b)). However, they are not in the same direction as $-\nabla T_e$ (Fig. 8 (c)). The electron density gradient was decreased by ECRH near $r_{eff} \sim 0.4$ m, and the electron density was higher at 20 ms after the start of ECRH injection than when ECRH began near the heating position $r_{eff} \sim 0.19$ m. Thus, the inward flux cannot be explained by the change in the density gradient. These results may indicate that the diffusion coefficient for the density gradient increased because the temperature was increased by ECRH. In addition, a positive radial electric field was generated at 0.2 m $< r_{eff} <$ 0.4 m by ECRH. It is possible that the positive radial electric field reduces the outward particle flux. From 8 ms after the ECRH injection, the inward flux was larger than the outward flux induced directly by ECRH. Consequently, the electron density increased in the core region starting 8 ms after ECRH injection beginning.

4.2 Density dependence of outward flux induced by ECRH shortly after heating

Density-ramp-up experiments were performed to clarify the parameter dependence of the flux induced shortly after the start of ECRH. The plasmas were sustained by NBI, and modulated ECRH was applied. Figure 9 shows the electron density and temperature measured by TS and the electron flux deduced by equation (2) with the electron density estimated by Abel-FIR. These are the values near the EC heating position ($r_{eff} \sim 0.19$ m). An outward electron flux was observed near the heating position shortly after the start of ECRH. Figure 10 presents the density dependence of the ECRH induced flux. $\Gamma_{ECRH,s}$ is the differ-

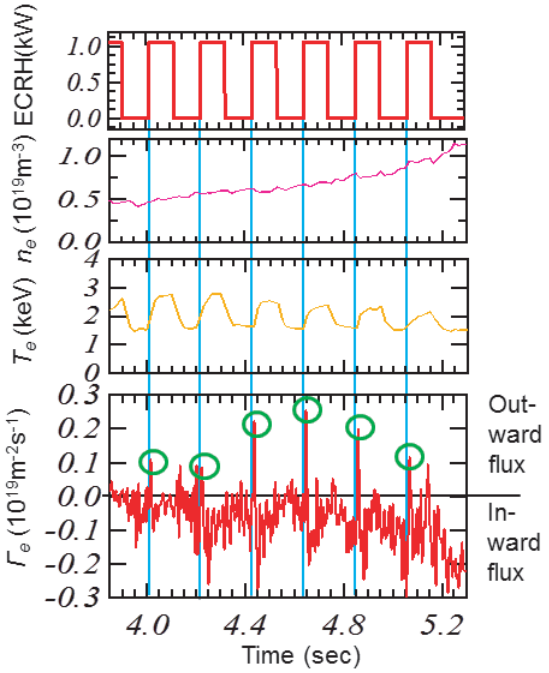

Fig. 9 Temporal evolution of ECRH injection power, electron density, temperature measured by TS, and the electron flux estimated using the electron density data measured by FIR-Abel near the heating position ($r_{\rm eff} \sim 0.19$ m).

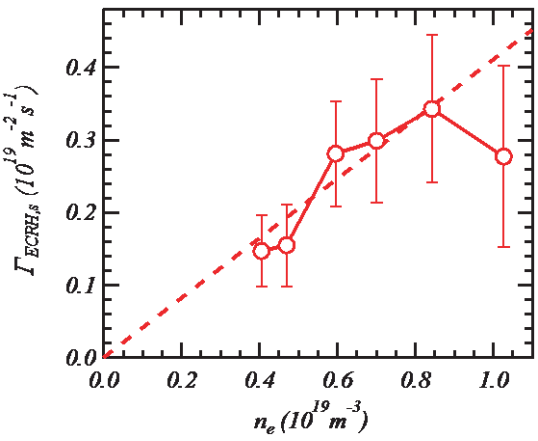

Fig. 10 Density dependence of electron flux shortly after ECRH injection near the heating position ($r_{\rm eff} \sim 0.19$ m).

ence between the peak value of the electron flux $\Gamma_{\rm e}$ shortly after the ECRH and the electron flux before the ECRH. The error bars for $\Gamma_{\rm ECRH,s}$ are estimated by considering the standard deviation of the electron density arising from the Abel transform of the line-integrated electron density measured by the FIR laser interferometers. $\Gamma_{\rm ECRH,s}$ is roughly proportional to the electron density in the density range of 0.4×10^{19} to 0.8×10^{19} m^{-3}. In the single-particle theory [4], the particle flux enhanced by the production of helically trapped particles is proportional to $n_{\rm e}^{-2}T_{\rm e}^{4}$ for the collision rate region of these plasmas. This electron flux $\Gamma_{\rm ECRH,s}$ cannot be expressed by the single-particle model for the flux enhanced by the transition from passing particles to helically trapped particles by ECRH. This indicates that either another model is needed for the effects of the production of trapped electrons induced by ECRH, or anomalous transport is dominant.

5. Summary

To observe the effects of the production of trapped particles, high-power ECRH was applied at the bottom of the ripple in the magnetic field strength in LHD. The temporal evolution of the electron density, temperature and the electric potential profiles were measured during high power EC heating. A rapid local decrease in the electron density and change in the electric potential to positive values were observed for 5 ms after the beginning of EC heating. This indicates that an outward electron flux is enhanced by ECRH. The rapid local outward electron flux induced by ECRH was first observed near the heating position shortly after the start of ECRH injection. The outward flux is approximately proportional to the electron density in the density range of 0.4×10^{19} to 0.8×10^{19} m^{-3}, and it cannot be explained by the single-particle theory for the flux enhanced by the transition from passing to helical trapped electrons caused by ECRH. Starting 8 ms after ECRH, an inward electron flux was observed in the core region. The main candidate for the cause of the inward electron flux is the increase in the diffusion coefficient of the density gradient and the generation of a positive radial electric field by ECRH.

Acknowledgment

The authors thank the ECRH and LHD staff for their discussions and for performing experiments.

[1] H. Idei *et al.*, Fusion Eng. Des. **26**, 167 (1995).
[2] H. Idei *et al.*, Phys. Rev. Lett. **71**, 2220 (1993).
[3] H. Sanuki *et al.*, J. Phys. Soc. Japan **69**, 445 (2000).
[4] K. Itoh *et al.*, J. Phys. Soc. Japan **58**, 482 (1989).
[5] C. Angioni *et al.*, Nucl. Fusion **44**, 827 (2004).
[6] S. Kubo *et al.*, Plasma Fusion Res. **3**, 1028 (2008).
[7] K. Tanaka *et al.*, Plasma Fusion Res. **3**, 050 (2008).
[8] H. Sanuki *et al.*, Phys. Scr. **52**, 461 (1995).
[9] V. Tribaldos, Phys. Plasmas **8**, 1229 (2001).